[5] ——, "On the existence of linear sliding surfaces for a class of uncertain dynamic systems with mismatched uncertainties," *Automatica*, vol. 35, pp. 1707–1715, 1999.
[6] R. H. C. Takahashi and P. L. D. Peres, "$\boldsymbol{H}_2$ guaranteed cost-switching surface design for sliding modes with nonmatching disturbances," *IEEE Trans. Autom. Control*, vol. 44, no. 11, pp. 2214–2218, Nov. 1999.
[7] K.-S. Kim, Y. Park, and S.-H. Oh, "Designing robust sliding hyperplnes for parametric uncertain systems: A Riccati approach," *Automatica*, vol. 36, pp. 1041–1048, 2000.
[8] H. H. Choi, "Variable structure output feedback control design for a class of uncertain dynamic systems," *Automatica*, vol. 38, pp. 335–341, 2001.
[9] ——, "An LMI-based switching surface design method for a class of mismatched uncertain systems," *IEEE Trans. Autom. Control*, vol. 48, no. 9, pp. 1634–1638, Sep. 2003.
[10] V. Utkin and J. Shi, "Integral sliding mode in systems operating under uncertainty conditions," in *Proc. 35th Conf. Decision Control*, Kobe, Japan, Dec. 1996, pp. 4591–4596.
[11] J. Ackermann and V. Utkin, "Sliding mode control design based on Ackermann's formula," *IEEE Trans. Autom. Control*, vol. 43, no. 2, pp. 234–237, Feb. 1998.
[12] W.-J. Cao and J.-X. Xu, "Nonlinear integral-type sliding surface for both matched and unmatched uncertain systems," *IEEE Trans. Autom. Control*, vol. 49, no. 8, pp. 1355–1360, Aug. 2004.
[13] A. Weinmann, *Uncertain Models and Robust Control*. New York: Springer-Verlag, 1991.
[14] S. Boyd, L. E. Ghaoui, E. Feron, and V. Balakrishnan, *Linear Matrix Inequalities in System and Control Theory*. Philadelphia, PA: SIAM, 1994.
[15] Y. Xia and Y. Jia, "Robust sliding-mode control of uncertain time-delay systems: An LMI approach," *IEEE Trans. Autom. Control*, vol. 48, no. 6, pp. 1086–1092, Jun. 2003.
[16] C. Edwards and S. K. Spurgeon, "Linear matrix inequality methods for designing sliding mode output feedback controllers," *Proc. Inst. Elect. Eng. Control Theory Appl.*, vol. 150, pp. 539–545, 2003.
[17] C. Scherer, P. Gahinet, and M. Chilali, "Multiobjective output-feedback control via LMI optimization," *IEEE Trans. Autom. Control*, vol. 42, no. 7, pp. 896–911, Jul. 1997.

Output Feedback Boundary Control of a Ginzburg–Landau Model of Vortex Shedding

Ole Morten Aamo, Andrey Smyshlyaev, Miroslav Krstić, and Bjarne A. Foss

***Abstract*—An exponentially convergent observer is designed for a linearized Ginzburg–Landau model of vortex shedding in viscous flow past a bluff body. Measurements are restricted to be taken collocated with the actuation which is applied on the cylinder surface. The observer is used in conjuction with a state feedback boundary controller designed in previous work to attenuate vortex shedding. While the theoretical results apply to the linearized system under sufficiently smooth initial data that satisfy the boundary conditions, simulations demonstrate the performance of the linear output feedback scheme on the nonlinear plant model.**

***Index Terms*—Backstepping, flow control, observers, partial differential equations.**

I. Introduction

The dynamics of the cylinder wake, often referred to as the von Kármán vortex street, is governed by the Navier–Stokes equation. However, in [7] and [17], a simplified model was suggested in the form of the complex Ginzburg–Landau equation

$$\frac{\partial A}{\partial t} = a_1 \frac{\partial^2 A}{\partial \breve{x}^2} + a_2 (\breve{x}) \frac{\partial A}{\partial \breve{x}} + a_3 (\breve{x}) A + a_4 |A|^2 A + \delta (\breve{x} - 1) u \quad (1)$$

where A is a complex-valued function of one spatial variable, $\breve{x} \in \mathbb{R}$, and time, $t \in \mathbb{R}_+$. The boundary conditions are $A(\pm\infty, t) = 0$. The control input, denoted u, is in the form of point actuation at the location of the cylinder, and the coefficients $a_i,\ i = 1, \ldots, 4$, were fitted to data from laboratory experiments in [17]. δ denotes the Dirac distribution. $A(\breve{x}, t)$ may represent any physical variable (velocities (u, v) or pressure p), or derivations thereof, along the centerline of the 2-D cylinder flow. The choice will have an impact on the performance of the Ginzburg–Landau model, and associating A with the transverse fluctuating velocity $v(\breve{x}, \breve{y} = 0, t)$ seems to be a particularly good choice [12]. As pointed out in [10], the model is derived for Reynolds numbers close to the critical Reynolds number for onset of vortex shedding, but has been shown to remain accurate far outside this vicinity for a wide variety of flows.

In [13], [17], it was shown numerically that the Ginzburg–Landau model for Reynolds numbers close to the critical Reynolds number for onset of vortex shedding can be stabilized using proportional feedback from a single measurement downstream of the cylinder, to local forcing at the location of the cylinder. Controllers for the Ginzburg–Landau model have previously been designed for finite dimensional approximations of (1) in [9] and [10] for the linearized model, and in [1] for the nonlinear model. Numerical investigations based on the Navier–Stokes

Manuscript received June 18, 2004; revised November 30, 2004, July 2, 2005, and July 10, 2006. Recommended by Associate Editor M. Demetriou. This work was supported by the National Science Foundation, by the Gas Technology Center NTNU, and by the Norwegian Research Council.

O. M. Aamo and B. A. Foss are with the Department of Engineering Cybernetics, NTNU, N-7491 Trondheim, Norway (e-mail: aamo@itk.ntnu.no).

A. Smyshlyaev and M. Krstić are with the Department of Mechanical and Aerospace Engineering, the University of California at San Diengo, La Jolla, CA 92093-0411 USA.

Digital Object Identifier 10.1109/TAC.2007.894544

equation are numerous, see for instance [14], [5], [6]. Lauga and Bewley [10] provides an excellent review of modelling aspects using (1), as well as an overview of previous work on stabilization of bluff body flows. We refer the reader to that reference for further details.

We consider here a simplification of (1). We linearize around the zero solution, discard the upstream subsystem by replacing the local forcing at $\breve{x} = 1$ with boundary input at this location, and truncate the downstream subsystem at some $x_d \in (-\infty, 1)$. Notice that the fluid flows in the negative $\breve{x}$ direction. We justify the truncation of the system by noting that the upstream subsystem is approximately uniform flow, whereas the downstream subsystem can be approximated to any desired level of accuracy by selecting x_d sufficiently far from the cylinder.[1] The resulting system is given by

$$\frac{\partial A}{\partial t} = a_1 \frac{\partial^2 A}{\partial \breve{x}^2} + a_2(\breve{x}) \frac{\partial A}{\partial \breve{x}} + a_3(\breve{x}) A \tag{2}$$

for $\breve{x} \in (x_d, 1)$, with boundary conditions

$$A(x_d, t) = 0, \text{ and } \left(A(1,t) = u(t) \text{ or } \frac{\partial A}{\partial \breve{x}}(1,t) = u(t) \right) \tag{3}$$

where $A : [x_d, 1] \times \mathbb{R}_+ \to \mathbb{C}$, $a_2 \in C^2([x_d, 1]; \mathbb{C})$, $a_3 \in C^1([x_d, 1]; \mathbb{C})$, $a_1 \in \mathbb{C}$, and $u : \mathbb{R}_+ \to \mathbb{C}$ is the control input. a_1 is assumed to have strictly positive real part. In [2], stabilizing state feedback boundary control laws for system (2)–(3) were derived based on the backstepping methodology [8]. The control laws made use of distributed measurements in a finite region downstream of the cylinder. In this note, we continue this work by restricting measurements to be taken at the location of the cylinder only, collocated with actuation, and solve the output feedback boundary control problem following the lines of [16]. Although the anticollocated case (with measurement taken in one point downstream of the cylinder) can also be solved by a similar procedure, we focus on the collocated case since it avoids the use of unrealistic mid-flow measurements. In order to implement the scheme in practice, transfer functions between the modelled Neumann actuation, $\partial A(1,t)/\partial \breve{x}$, and the physical actuation, and the physical sensing and the modelled sensing, $A(1,t)$, would have to be determined, either experimentally or computationally. The physical actuation could for instance be micro/synthetic jet actuators distributed on the cylinder surface, and a possible choice for the physical sensing could be pressure sensors distributed on the cylinder surface. For further background material, see [3], [11], [15], [2], [16], and the references therein.

II. Problem Statement

We now rewrite the equation to obtain two coupled partial differential equations in real variables and coefficients by defining $\rho(x,t) = \Re(B(x,t)) = \left(B(x,t) + \bar{B}(x,t)\right)/2$, and $\iota(x,t) = \Im(B(x,t)) = \left(B(x,t) - \bar{B}(x,t)\right)/(2i)$, where $x = (\breve{x} - x_d)/(1 - x_d)$, $B(x,t) = A(\breve{x},t) \exp\left((1/2a_1)\int_{x_d}^{\breve{x}} a_2(\tau)\, d\tau\right)$, i denotes the imaginary unit, and $\bar{}$ denotes complex conjugation. Equation (2) becomes

$$\begin{aligned} \rho_t &= a_R \rho_{xx} + b_R(x)\rho - a_I \iota_{xx} - b_I(x)\iota \\ \iota_t &= a_I \rho_{xx} + b_I(x)\rho + a_R \iota_{xx} + b_R(x)\iota \end{aligned} \tag{4}$$

for $x \in (0,1)$, with boundary conditions

$$\rho(0,t) = 0,\ \iota(0,t) = 0, \text{ and} \tag{5}$$

$$\begin{aligned} \rho(1,t) &= u_R(t),\ \iota(1,t) = u_I(t), \text{ or} \\ \rho_x(1,t) &= u_R(t),\ \iota_x(1,t) = u_I(t) \end{aligned} \tag{6}$$

where $a_R \triangleq \Re(a_1)/(1 - x_d)^2$, $a_I \triangleq \Im(a_1)/(1 - x_d)^2$, and

$$\begin{aligned} b_R(x) &\triangleq \Re\left(a_3(\breve{x}) - \frac{1}{2}a_2'(\breve{x}) - \frac{1}{4a_1}a_2^2(\breve{x})\right) \\ b_I(x) &\triangleq \Im\left(a_3(\breve{x}) - \frac{1}{2}a_2'(\breve{x}) - \frac{1}{4a_1}a_2^2(\breve{x})\right). \end{aligned} \tag{7}$$

The problem is to find a convergent observer for (4)–(6) with only boundary measurements available, and use it in conjunction with the state feedback control law found in [2] to derive stabilizing output feedback boundary control laws. The observer design relates to the state feedback problem solved in [2] in a way reminiscent of the duality of the corresponding problems for finite dimensional systems. Thus, we start by reviewing the results in [2].

III. Stabilization by State Feedback

In [2], extending the results in [11] and [15], the state feedback stabilization problem was solved by searching for a coordinate transformation in the form

$$\breve{\rho}(x,t) = \rho(x,t) - \int_0^x \left[k(x,y)\rho(y,t) + k_c(x,y)\iota(y,t)\right] dy \tag{8}$$

$$\breve{\iota}(x,t) = \iota(x,t) - \int_0^x \left[-k_c(x,y)\rho(y,t) + k(x,y)\iota(y,t)\right] dy \tag{9}$$

transforming system (4)–(6) into

$$\begin{aligned} \breve{\rho}_t &= a_R \breve{\rho}_{xx} + f_R(x)\breve{\rho} - a_I \breve{\iota}_{xx} - f_I(x)\breve{\iota} \\ \breve{\iota}_t &= a_I \breve{\rho}_{xx} + f_I(x)\breve{\rho} + a_R \breve{\iota}_{xx} + f_R(x)\breve{\iota} \end{aligned} \tag{10}$$

for $x \in (0,1)$, with boundary conditions

$$\begin{aligned} &\breve{\rho}(0,t) = \breve{\iota}(0,t) = 0, \text{ and} \\ &\breve{\rho}(1,t) = \breve{\iota}(1,t) = 0, \text{ or } \breve{\rho}_x(1,t) = \breve{\iota}_x(1,t) = 0. \end{aligned} \tag{11}$$

By the choice of f_R and f_I, system (10)–(11) can be given any desired level of stability. The corresponding stable behaviour for the original system is ensured by the control input

$$u_R(t) = \int_0^1 \left[k_1(y)\rho(y,t) + k_{c,1}(y)\iota(y,t)\right] dy \tag{12}$$

$$u_I(t) = \int_0^1 \left[-k_{c,1}(y)\rho(y,t) + k_1(y)\iota(y,t)\right] dy \tag{13}$$

for Dirichlet actuation, where $k_1(y) = k(1,y)$, $k_{c,1}(y) = k_c(1,y)$, and

$$\begin{aligned} u_R(t) = &\int_0^1 \left[k_2(y)\rho(y,t) + k_{c,2}(y)\iota(y,t)\right] dy \\ &+ k_1(1)\rho(1,t) + k_{c,1}(1)\iota(1,t) \end{aligned} \tag{14}$$

$$\begin{aligned} u_I(t) = &\int_0^1 \left[-k_{c,2}(y)\rho(y,t) + k_2(y)\iota(y,t)\right] dy \\ &- k_{c,1}(1)\rho(1,t) + k_1(1)\iota(1,t) \end{aligned} \tag{15}$$

for Neumann actuation, where $k_2(y) = k_x(1,y)$, $k_{c,2}(y) = k_{c,x}(1,y)$. The skew-symmetric form of (12)–(13) and (14)–(15) is postulated from the skew-symmetric form of (4). The following result

[1] This claim is postulated from the observation that the local damping effect in (1) increases with increasing distance from the cylinder, which follows from the coefficients reported in [17].

was proven in [2][2] for the Dirichlet controller (12)–(13) (it is valid also for the Neumann controller (14)–(15), as stated here).

Theorem 1:

i) The pair of kernels, $k(x,y)$ and $k_c(x,y)$, satisfy the partial differential equation

$$\begin{aligned} k_{xx} &= k_{yy} + \beta(x,y)k + \beta_c(x,y)k_c \\ k_{c,xx} &= k_{c,yy} - \beta_c(x,y)k + \beta(x,y)k_c \end{aligned} \tag{16}$$

for $(x,y) \in \mathcal{T} = \{x, y : 0 < y < x < 1\}$, with boundary conditions

$$\begin{aligned} k(x,x) &= -\frac{1}{2}\int_0^x \beta(\gamma,\gamma)d\gamma,\ k(x,0) = 0 \\ k_c(x,x) &= \frac{1}{2}\int_0^x \beta_c(\gamma,\gamma)d\gamma,\ k_c(x,0) = 0 \end{aligned} \tag{17}$$

where

$$\beta(x,y) = \frac{a_R\left(b_R(y) - f_R(x)\right) + a_I\left(b_I(y) - f_I(x)\right)}{a_R^2 + a_I^2} \tag{18}$$

$$\beta_c(x,y) = \frac{a_R\left(b_I(y) - f_I(x)\right) - a_I\left(b_R(y) - f_R(x)\right)}{a_R^2 + a_I^2}. \tag{19}$$

Equation (16) with boundary conditions (17) has a unique $C^2(\mathcal{T})$ solution, given by

$$\begin{aligned} k(x,y) &= \sum_{n=0}^{\infty} G_n(x+y, x-y) \\ k_c(x,y) &= \sum_{n=0}^{\infty} G_{c,n}(x+y, x-y) \end{aligned} \tag{20}$$

where

$$G_0(\xi,\eta) = -\frac{1}{4}\int_\eta^\xi b(\tau,0)\,d\tau,\ G_{c,0}(\xi,\eta) = \frac{1}{4}\int_\eta^\xi b_c(\tau,0)\,d\tau \tag{21}$$

$$\begin{aligned} G_{n+1}(\xi,\eta) = &\frac{1}{4}\int_\eta^\xi \int_0^\eta b(\tau,s)\,G_n(\tau,s)\,ds d\tau \\ &+ \frac{1}{4}\int_\eta^\xi \int_0^\eta b_c(\tau,s)\,G_{c,n}(\tau,s)\,ds d\tau \end{aligned} \tag{22}$$

$$\begin{aligned} G_{c,n+1}(\xi,\eta) = &-\frac{1}{4}\int_\eta^\xi \int_0^\eta b_c(\tau,s)\,G_n(\tau,s)\,ds d\tau \\ &+ \frac{1}{4}\int_\eta^\xi \int_0^\eta b(\tau,s)\,G_{c,n}(\tau,s)\,ds d\tau \end{aligned} \tag{23}$$

and

$$b(\xi,\eta) = \beta\left(\frac{\xi+\eta}{2}, \frac{\xi-\eta}{2}\right),\ b_c(\xi,\eta) = \beta_c\left(\frac{\xi+\eta}{2}, \frac{\xi-\eta}{2}\right). \tag{24}$$

ii) The inverse of (8)–(9) exists and is in the form

$$\rho(x,t) = \breve{\rho}(x,t) - \int_0^x \left[l(x,y)\,\breve{\rho}(y,t) + l_c(x,y)\,\breve{\iota}(y,t)\right] dy \tag{25}$$

$$\iota(x,t) = \breve{\iota}(x,t) - \int_0^x \left[-l_c(x,y)\,\breve{\rho}(y,t) + l(x,y)\,\breve{\iota}(y,t)\right] dy \tag{26}$$

[2]In the statement of Theorem 1 and in the text in [2, Sec. 8], $\boldsymbol{L_\infty(0,1)}$ should be replaced by $\boldsymbol{H_3(0,1)}$. Furthermore, the initial conditions must be compatible with the boundary conditions.

where l and l_c are $C^2(\mathcal{T})$ functions. l and l_c can be expressed similarly to k and k_c in (20)–(23), but we omit their explicit definition due to page limitations.

iii) Suppose $c > 0$, and select f_R and f_I such that

$$\sup_{x\in[0,1]}\left(f_R(x) + \frac{1}{2}\left|f_I'(x)\right|\right) \le -c. \tag{27}$$

Then for any initial data $(\rho_0, \iota_0) \in H_3(0,1)$, compatible with the boundary conditions, the system (4)–(6) in closed loop with the control law (12)–(13) has a unique classical solution $(\rho,\iota) \in C^{2,1}((0,1)\times(0,\infty))$ and is exponentially stable at the origin in the $L_2(0,1)$ and $H_1(0,1)$ norms. If, in addition, $f_R'(1) = f_I'(1) = 0$, then the same conclusion holds for the control law (14)–(15).

In [2], it was shown that a particular choice of f_R and f_I, that depend on x_d in a specific way, results in state feedback kernel functions that are invariant of x_d and vanish in $[x_d, x_s]$, where x_s is a constant that can be deduced from the coefficients of (1). This implies that if the domain is truncated at some $x_d \le x_s$ for the purpose of computing the feedback kernel functions, the resulting state feedback will stabilize the plant evolving on the semi-infinite domain $(-\infty, 1)$. This is achieved by avoiding the complete cancellation of the terms involving b_R and b_I in (4) by using a target system (10) that contains the natural damping that exists in the plant downstream of x_s. It ensures that only cancellation/domination of the source of instability is performed in the design, and is similar to common practice in design of finite dimensional backstepping controllers, where one seeks to leave unaltered terms that add to the stability while cancelling terms that do not. The result is less complexity, and better robustness properties. The significance of this with regard to the present work, is that we need to design an observer that provides an estimate of the state in the interval $[x_s, 1]$, only. In the anticollocated case, placing the measurement at x_s, the observer can be designed on $[x_s, 1]$ and guarantee output feedback stabilization on the semi-infinite domain $(-\infty, 1)$. In the collocated case, stability is guaranteed when the system is truncated to a finite domain. An interesting property of our design is that it requires the solution of a linear hyperbolic PDE, which is an advantage when compared to other methods, such as LQG requiring the solution of a Riccati equation, which is quadratic. In fact, for a plant much simpler than the linearized Ginzburg–Landau model, solving the hyperbolic PDE is reported in [15] to take an order of magnitude less computational time than solving the Riccati equation. Although the series (20) happen to converge rapidly, they can be computed by a more efficient numerical scheme that was developed in [15].

IV. Observer Design

In the collocated case, measurements are taken at the same location as the control input, that is on the cylinder surface. The measurements are $y_R(t) = \rho(1,t)$ and $y_I(t) = \iota(1,t)$, which leaves $\rho_x(1,t)$ and $\iota_x(1,t)$ for control input. Consider the following Luenberger type observer (omitting the independent variable t for notational brevity)

$$\begin{aligned} \hat{\rho}_t = &a_R\hat{\rho}_{xx} + b_R(x)\,\hat{\rho} - a_I\hat{\iota}_{xx} - b_I(x)\,\hat{\iota} \\ &+ p_1(x)\left(y_R - \hat{y}_R\right) + p_{c,1}(x)\left(y_I - \hat{y}_I\right) \end{aligned} \tag{28}$$

$$\begin{aligned} \hat{\iota}_t = &a_I\hat{\rho}_{xx} + b_I(x)\,\hat{\rho} + a_R\hat{\iota}_{xx} + b_R(x)\,\hat{\iota} \\ &- p_{c,1}(x)\left(y_R - \hat{y}_R\right) + p_1(x)\left(y_I - \hat{y}_I\right) \end{aligned} \tag{29}$$

for $x \in (0,1)$, with boundary conditions $\hat{\rho}(0) = \hat{\iota}(0) = 0$ and

$$\hat{\rho}_x(1) = p_0\left(\rho(1) - \hat{\rho}(1)\right) + p_{c,0}\left(\iota(1) - \hat{\iota}(1)\right) + u_R \tag{30}$$

$$\hat{\iota}_x(1) = -p_{c,0}\left(\rho(1) - \hat{\rho}(1)\right) + p_0\left(\iota(1) - \hat{\iota}(1)\right) + u_I. \tag{31}$$

In (28)–(31), $p_1(x)$, $p_{c,1}(x)$, p_0 and $p_{c,0}$ are output injection gains to be designed. Defining the observer error $\tilde{\rho}(x) = \rho(x) - \hat{\rho}(x)$, $\tilde{\iota}(x) = \iota(x) - \hat{\iota}(x)$, the error dynamics are given by

$$\begin{aligned}\tilde{\rho}_t &= a_R\tilde{\rho}_{xx} + b_R(x)\tilde{\rho} - a_I\tilde{\iota}_{xx} - b_I(x)\tilde{\iota} \\ &\quad - p_1(x)\tilde{\rho}(1) - p_{c,1}(x)\tilde{\iota}(1) \qquad (32)\\ \tilde{\iota}_t &= a_I\tilde{\rho}_{xx} + b_I(x)\tilde{\rho} + a_R\tilde{\iota}_{xx} + b_R(x)\tilde{\iota} \\ &\quad + p_{c,1}(x)\tilde{\rho}(1) - p_1(x)\tilde{\iota}(1) \qquad (33)\end{aligned}$$

for $x \in (0,1)$, with boundary conditions $\tilde{\rho}(0) = \tilde{\iota}(0) = 0$ and

$$\tilde{\rho}_x(1) = -p_0\tilde{\rho}(1) - p_{c,0}\tilde{\iota}(1),\ \tilde{\iota}_x(1) = p_{c,0}\tilde{\rho}(1) - p_0\tilde{\iota}(1). \quad (34)$$

The output injection gains $p_1(x)$, $p_{c,1}(x)$, p_0 and $p_{c,0}$ should be chosen to stabilize the system (32)–(34). Towards that end, we look for a transformation

$$\tilde{\rho}(x,t) = \tilde{\sigma}(x,t) - \int_x^1 \left[p(x,y)\tilde{\sigma}(y,t) + p_c(x,y)\tilde{\kappa}(y,t)\right]dy \quad (35)$$

$$\tilde{\iota}(x,t) = \tilde{\kappa}(x,t) - \int_x^1 \left[-p_c(x,y)\tilde{\sigma}(y,t) + p(x,y)\tilde{\kappa}(y,t)\right]dy \quad (36)$$

that transforms system (32)–(34) into the exponentially stable system

$$\begin{aligned}\tilde{\sigma}_t &= a_R\tilde{\sigma}_{xx} + f_R(x)\tilde{\sigma} - a_I\tilde{\kappa}_{xx} - f_I(x)\tilde{\kappa} \\ \tilde{\kappa}_t &= a_I\tilde{\sigma}_{xx} + f_I(x)\tilde{\sigma} + a_R\tilde{\kappa}_{xx} + f_R(x)\tilde{\kappa}\end{aligned} \quad (37)$$

for $x \in (0,1)$, with boundary conditions

$$\tilde{\sigma}(0) = \tilde{\kappa}(0) = 0,\ \tilde{\sigma}_x(1) = \tilde{\kappa}_x(1) = 0. \quad (38)$$

When the transformation is found, the output injection gains are given by

$$p_1(x) = -a_R p_y(x,1) - a_I p_{c,y}(x,1),\ p_0 = -p(1,1) \quad (39)$$

$$p_{c,1}(x) = a_I p_y(x,1) - a_R p_{c,y}(x,1),\ p_{c,0} = -p_c(1,1). \quad (40)$$

By subtracting (32)–(34) from (37) and (38), and using (35) and (36), it can be shown that the kernels $p(x,y)$ and $p_c(x,y)$ must satisfy

$$\begin{aligned}p_{xx} &= p_{yy} - \bar{\beta}(x,y)p - \bar{\beta}_c(x,y)p_c \\ p_{c,xx} &= p_{c,yy} + \bar{\beta}_c(x,y)p - \bar{\beta}(x,y)p_c\end{aligned} \quad (41)$$

with boundary conditions

$$\begin{aligned}p(x,x) &= -\frac{1}{2}\int_0^x \bar{\beta}(\gamma,\gamma)\,d\gamma,\ p(0,y) = 0 \\ p_c(x,x) &= \frac{1}{2}\int_0^x \bar{\beta}_c(\gamma,\gamma)\,d\gamma,\ p_c(0,y) = 0\end{aligned} \quad (42)$$

where

$$\bar{\beta}(x,y) = \frac{a_R(b_R(x) - f_R(y)) + a_I(b_I(x) - f_I(y))}{a_R^2 + a_I^2} \quad (43)$$

$$\bar{\beta}_c(x,y) = \frac{a_R(b_I(x) - f_I(y)) - a_I(b_R(x) - f_R(y))}{a_R^2 + a_I^2}. \quad (44)$$

Changing coordinates according to $\breve{x} = y$, $\breve{y} = x$, defining $\breve{p}(\breve{x},\breve{y}) \triangleq p(x,y)$, $\breve{p}_c(\breve{x},\breve{y}) \triangleq p_c(x,y)$, and noticing that $\bar{\beta}(\breve{y},\breve{x}) = \beta(\breve{x},\breve{y})$ and $\bar{\beta}_c(\breve{y},\breve{x}) = \beta_c(\breve{x},\breve{y})$, we obtain

$$\begin{aligned}\breve{p}_{\breve{x}\breve{x}} &= \breve{p}_{\breve{y}\breve{y}} + \beta(\breve{x},\breve{y})\breve{p} + \beta_c(\breve{x},\breve{y})\breve{p}_c \\ \breve{p}_{c,\breve{x}\breve{x}} &= \breve{p}_{c,\breve{y}\breve{y}} - \beta_c(\breve{x},\breve{y})\breve{p} + \beta(\breve{x},\breve{y})\breve{p}_c\end{aligned} \quad (45)$$

with boundary conditions

$$\begin{aligned}\breve{p}(\breve{x},\breve{x}) &= -\frac{1}{2}\int_0^{\breve{x}} \beta(\gamma,\gamma)\,d\gamma,\ \breve{p}(\breve{x},0) = 0 \\ \breve{p}_c(\breve{x},\breve{x}) &= \frac{1}{2}\int_0^{\breve{x}} \beta_c(\gamma,\gamma)\,d\gamma,\ \breve{p}_c(\breve{x},0) = 0.\end{aligned} \quad (46)$$

From (39) and (40), we have $\breve{p}_1(\breve{y}) = -a_R\breve{p}_{\breve{x}}(1,\breve{y}) - a_I\breve{p}_{c,\breve{x}}(1,\breve{y})$, $\breve{p}_{c,1}(\breve{y}) = a_I\breve{p}_{\breve{x}}(1,\breve{y}) - a_R\breve{p}_{c,\breve{x}}(1,\breve{y})$, $p_0 = -\breve{p}(1,1)$, and $p_{c,0} = -\breve{p}_c(1,1)$. Since (45) and (46) is identical with (16) and (17), it follows that the output injection gains can be obtained from the state feedback gains as

$$\begin{aligned}p_1(x) &= -a_R k_x(1,x) - a_I k_{c,x}(1,x) \\ p_{c,1}(x) &= a_I k_x(1,x) - a_R k_{c,x}(1,x)\end{aligned} \quad (47)$$

$$p_0 = -k(1,1),\ p_{c,0} = -k_c(1,1) \quad (48)$$

and we get the following result directly from Theorem 1.

Theorem 2: Suppose f_R and f_I satisfy (27) and $f_R'(1) = f_I'(1) = 0$, and let k, k_c be the solution of (16)–(17). Then for any initial data $(\tilde{\rho}_0, \tilde{\iota}_0) \in H_3(0,1)$, compatible with the boundary conditions, the system (32)–(34) with output injection gains given by (47)–(48) has a unique classical solution $(\tilde{\rho}, \tilde{\iota}) \in C^{2,1}((0,1)\times(0,\infty))$ and is exponentially stable at the origin in the $L_2(0,1)$ and $H_1(0,1)$ norms.

V. Output Feedback Control Design

The state feedback control law presented in Section III can be implemented by replacing $\rho(y,t)$ and $\iota(y,t)$ by their estimates $\hat{\rho}(y,t)$ and $\hat{\iota}(y,t)$ in (14) and (15). This adds the dynamics of the observer into the feedback loop, and we need to verify that closed loop stability is preserved. We formulate the solution to the ouput-feedback problem as follows.

Theorem 3: Suppose f_R and f_I satisfy (27) and $f_R'(1) = f_I'(1) = 0$, and let k, k_c be the solution of (16)–(17). Then for any initial data $(\rho_0, \iota_0, \hat{\rho}_0, \hat{\iota}_0) \in H_3(0,1)$, compatible with the boundary conditions, system (4)–(5) with the controller

$$\begin{aligned}\rho_x(1) &= \int_0^1 \left[k_x(1,y)\hat{\rho}(y) + k_{c,x}(1,y)\hat{\iota}(y)\right]dy \\ &\quad + k(1,1)\rho(1) + k_c(1,1)\iota(1) \qquad (49)\\ \iota_x(1) &= \int_0^1 \left[-k_{c,x}(1,y)\hat{\rho}(y) + k_x(1,y)\hat{\iota}(y)\right]dy \\ &\quad - k_c(1,1)\rho(1) + k(1,1)\iota(1) \qquad (50)\end{aligned}$$

and the observer

$$\begin{aligned}\hat{\rho}_t &= a_R\hat{\rho}_{xx} + b_R(x)\hat{\rho} - a_I\hat{\iota}_{xx} - b_I(x)\hat{\iota} \\ &\quad + p_1(x)(\rho(1) - \hat{\rho}(1)) + p_{c,1}(x)(\iota(1) - \hat{\iota}(1)) \qquad (51)\\ \hat{\iota}_t &= a_I\hat{\rho}_{xx} + b_I(x)\hat{\rho} + a_R\hat{\iota}_{xx} + b_R(x)\hat{\iota} \\ &\quad - p_{c,1}(x)(\rho(1) - \hat{\rho}(1)) + p_1(x)(\iota(1) - \hat{\iota}(1)) \qquad (52)\end{aligned}$$

$$\hat{\rho}(0)=0,\ \hat{\iota}(0)=0 \tag{53}$$

$$\hat{\rho}_x(1)=p_0(\rho(1)-\hat{\rho}(1))+p_{c,0}(\iota(1)-\hat{\iota}(1))+\rho_x(1) \tag{54}$$

$$\hat{\iota}_x(1)=-p_{c,0}(\rho(1)-\hat{\rho}(1))+p_0(\iota(1)-\hat{\iota}(1))+\iota_x(1) \tag{55}$$

has unique classical solutions $(\rho,\iota,\hat{\rho},\hat{\iota})\in C^{2,1}((0,1)\times(0,\infty))$ and is exponentially stable at the origin in the $L_2(0,1)$ and $H_1(0,1)$ norms.

Proof: The coordinate transformation

$$\hat{\sigma}(x,t)=\hat{\rho}(x,t)-\int_0^x\left[k(x,y)\hat{\rho}(y,t)+k_c(x,y)\hat{\iota}(y,t)\right]dy \tag{56}$$

$$\hat{\kappa}(x,t)=\hat{\iota}(x,t)-\int_0^x\left[-k_c(x,y)\hat{\rho}(y,t)+k(x,y)\hat{\iota}(y,t)\right]dy \tag{57}$$

maps (51)–(55) into the system

$$\hat{\sigma}_t=a_R\hat{\sigma}_{xx}+f_R(x)\hat{\sigma}-a_I\hat{\kappa}_{xx}-f_I(x)\hat{\kappa}-\gamma(x)\tilde{\sigma}(1)-\gamma_c(x)\tilde{\kappa}(1) \tag{58}$$

$$\hat{\kappa}_t=a_I\hat{\sigma}_{xx}+f_I(x)\hat{\sigma}+a_R\hat{\kappa}_{xx}+f_R(x)\hat{\kappa}+\gamma_c(x)\tilde{\sigma}(1)-\gamma(x)\tilde{\kappa}(1) \tag{59}$$

for $x\in(0,1)$, with boundary conditions

$$\hat{\sigma}(0,t)=\hat{\kappa}(0,t)=0,\ \hat{\sigma}_x(1,t)=\hat{\kappa}_x(1,t)=0 \tag{60}$$

where

$$\gamma(x)=\int_0^x\left[k(x,y)p_1(y)-k_c(x,y)p_{c,1}(y)\right]dy \tag{61}$$

$$\gamma_c(x)=\int_0^x\left[k(x,y)p_{c,1}(y)+k_c(x,y)p_1(y)\right]dy. \tag{62}$$

Notice that systems (37) and (38) and (58)–(60) form a cascade, where the $(\hat{\sigma},\hat{\kappa})$ subsystem is driven by the $(\tilde{\sigma},\tilde{\kappa})$ subsystem. Well posedness of the $(\tilde{\sigma},\tilde{\kappa})$ subsystem is established in Theorem 2. From standard results for uniformly parabolic equations (see, e.g., [4]; system (58)–(60) is uniformly parabolic in (0, 1), with module of parabolicity a_R) it follows that system (58)–(59) with boundary conditions (60) and initial data $\hat{\sigma}_0,\hat{\kappa}_0\in H_3(0,1)$, has a unique classical solution $\hat{\sigma},\hat{\kappa}\in C^{2,1}((0,1)\times(0,\infty))$. The smoothness of k,k_c and of the kernels for the inverse transformation, l,l_c, as stated in Theorem 1, provide well posedness of system (4)–(5) in closed loop with (49)–(55). Next, we establish stability. Let $\|\cdot\|$ denote the $L_2(0,1)$ norm, and consider

$$E(t)=\frac{1}{2}\int_0^1\left(\hat{\sigma}^2+\hat{\kappa}^2+\mu\tilde{\sigma}^2+\mu\tilde{\kappa}^2\right)dx=\frac{1}{2}\left(\|\hat{\sigma}\|^2+\|\hat{\kappa}\|^2+\mu\|\tilde{\sigma}\|^2+\mu\|\tilde{\kappa}\|^2\right) \tag{63}$$

where μ is a strictly positive constant to be determined. Due to (27), the time derivative of $E(t)$ along solutions of system (37) and (38) and (58)–(60) satisfies

$$\dot{E}(t)\le -cE(t)-\frac{c}{2}\left(\|\hat{\sigma}\|^2+\|\hat{\kappa}\|^2+\mu\|\tilde{\sigma}\|^2+\mu\|\tilde{\kappa}\|^2\right)+\bar{\gamma}\int_0^1\left(|\hat{\sigma}\tilde{\sigma}(1)|+|\hat{\sigma}\tilde{\kappa}(1)|+|\hat{\kappa}\tilde{\sigma}(1)|+|\hat{\kappa}\tilde{\kappa}(1)|\right)dx-a_R\|\hat{\sigma}_x\|^2-a_R\|\hat{\kappa}_x\|^2-\mu a_R\|\tilde{\sigma}_x\|^2-\mu a_R\|\tilde{\kappa}_x\|^2 \tag{64}$$

where $\bar{\gamma}\triangleq\max\left\{\sup_{x\in[0,1]}|\gamma(x)|,\sup_{x\in[0,1]}|\gamma_c(x)|\right\}$. Using Schwartz' inequality twice, along with (38), we have $\int_0^1|\hat{\sigma}\tilde{\sigma}(1)|dx\le\|\hat{\sigma}\|\|\tilde{\sigma}_x\|$, and similarly for the other terms appearing in the integrand in the right hand side of (64), so upon completion of squares we get

$$\begin{aligned}\dot{E}(t)\le&-cE(t)-\left(\frac{\sqrt{c}}{2}\|\hat{\sigma}\|-\frac{\bar{\gamma}}{\sqrt{c}}\|\tilde{\sigma}_x\|\right)^2-\left(\frac{\sqrt{c}}{2}\|\hat{\sigma}\|-\frac{\bar{\gamma}}{\sqrt{c}}\|\tilde{\kappa}_x\|\right)^2-\left(\frac{\sqrt{c}}{2}\|\hat{\kappa}\|-\frac{\bar{\gamma}}{\sqrt{c}}\|\tilde{\sigma}_x\|\right)^2\\&-\left(\frac{\sqrt{c}}{2}\|\hat{\kappa}\|-\frac{\bar{\gamma}}{\sqrt{c}}\|\tilde{\kappa}_x\|\right)^2+\left(2\frac{\bar{\gamma}^2}{c}-\mu a_R\right)\left(\|\tilde{\sigma}_x\|^2+\|\tilde{\kappa}_x\|^2\right).\end{aligned} \tag{65}$$

Setting $\mu=2\bar{\gamma}^2/(ca_R)$, and applying the comparison principle, we obtain

$$E(t)\le E(0)e^{-ct} \tag{66}$$

which proves exponential stability of the $(\hat{\sigma},\hat{\kappa},\tilde{\sigma},\tilde{\kappa})$-system in the $L_2(0,1)$ norm. Next, consider

$$V(t)=\frac{1}{2}\int_0^1\left(\hat{\sigma}_x^2+\hat{\kappa}_x^2+\mu\tilde{\sigma}_x^2+\mu\tilde{\kappa}_x^2\right)dx=\frac{1}{2}\left(\|\hat{\sigma}_x\|^2+\|\hat{\kappa}_x\|^2+\mu\|\tilde{\sigma}_x\|^2+\mu\|\tilde{\kappa}_x\|^2\right). \tag{67}$$

Due to (27), the derivative of $V(t)$ along solutions of system (37)–(38) and (58)–(60) satisfies

$$\begin{aligned}\dot{V}(t)\le&-a_R\left(\|\hat{\sigma}_{xx}\|^2+\|\hat{\kappa}_{xx}\|^2+\mu\|\tilde{\sigma}_{xx}\|^2+\mu\|\tilde{\kappa}_{xx}\|^2\right)\\&+\bar{\gamma}(\|\hat{\sigma}_{xx}\|\|\tilde{\sigma}_x\|+\|\hat{\sigma}_{xx}\|\|\tilde{\kappa}_x\|+\|\hat{\kappa}_{xx}\|\|\tilde{\sigma}_x\|+\|\hat{\kappa}_{xx}\|\|\tilde{\kappa}_x\|)\\&-\frac{3c}{4}\left(\|\hat{\sigma}_x\|^2+\|\hat{\kappa}_x\|^2+\mu\|\tilde{\sigma}_x\|^2+\mu\|\tilde{\kappa}_x\|^2\right)\\&+\frac{2}{c}\int_0^1\left(f_R'(x)^2+f_I'(x)^2\right)\left(\hat{\sigma}^2+\hat{\kappa}^2+\mu\tilde{\sigma}^2+\mu\tilde{\kappa}^2\right)dx.\end{aligned} \tag{68}$$

Defining $c_2=4\sup_{x\in[0,1]}\left\{f_R'(x)^2+f_I'(x)^2\right\}/c$, we have

$$\begin{aligned}\dot{V}(t)\le&-\frac{c}{2}V(t)+c_2E(t)\\&-a_R\left(\|\hat{\sigma}_{xx}\|^2+\|\hat{\kappa}_{xx}\|^2+\mu\|\tilde{\sigma}_{xx}\|^2+\mu\|\tilde{\kappa}_{xx}\|^2\right)\\&+\bar{\gamma}(\|\hat{\sigma}_{xx}\|\|\tilde{\sigma}_x\|+\|\hat{\sigma}_{xx}\|\|\tilde{\kappa}_x\|+\|\hat{\kappa}_{xx}\|\|\tilde{\sigma}_x\|+\|\hat{\kappa}_{xx}\|\|\tilde{\kappa}_x\|)\\&-\frac{c}{2}\left(\|\hat{\sigma}_x\|^2+\|\hat{\kappa}_x\|^2+\mu\|\tilde{\sigma}_x\|^2+\mu\|\tilde{\kappa}_x\|^2\right).\end{aligned} \tag{69}$$

Completing squares, using (66), and applying the comparison principle, we obtain $V(t)\le(V(0)+2c_2E(0)/c)e^{-(c/2)t}$. From the Poincaré inequality, $E\le V/2$, we get

$$V(t)\le\left(1+\frac{c_2}{c}\right)V(0)e^{-(c/2)t} \tag{70}$$

which proves exponential stability of the $(\hat{\sigma},\hat{\kappa},\tilde{\sigma},\tilde{\kappa})$-system in $H_1(0,1)$. Since transformation (56)–(57) and its inverse imply equivalence of norms of $(\hat{\rho},\hat{\iota},\tilde{\rho},\tilde{\iota})$ and $(\hat{\sigma},\hat{\kappa},\tilde{\sigma},\tilde{\kappa})$ in $L_2(0,1)$ and $H_1(0,1)$, the properties proven for system (58)–(60) also hold for system (51)–(55). Since $(\hat{\rho},\hat{\iota},\tilde{\rho},\tilde{\iota})$ is exponentially stable at the origin in $L_2(0,1)$ and $H_1(0,1)$, so is $(\hat{\rho},\hat{\iota},\rho,\iota)$. ■

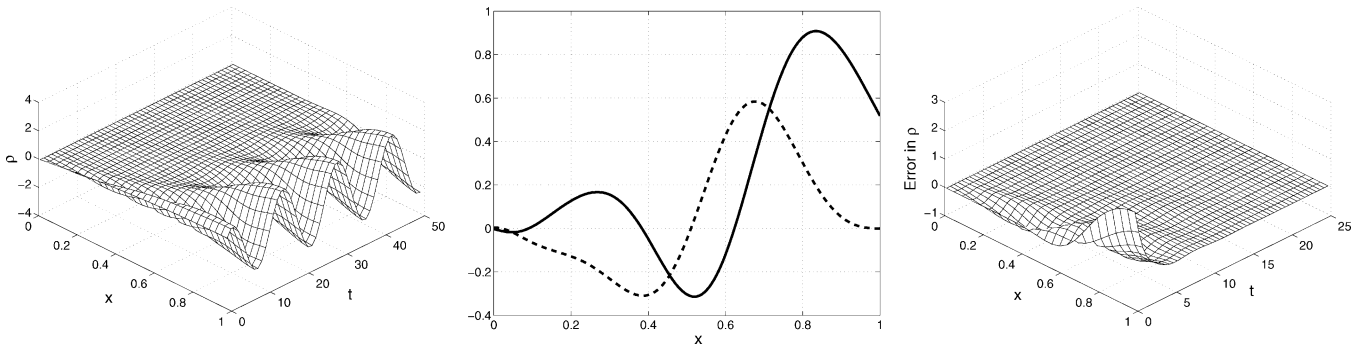

Fig. 1. Left graph: Open-loop simulation of nonlinear system. Middle graph: Output injection gains $\boldsymbol{p}_1(\boldsymbol{x})$ (solid) and $\boldsymbol{p}_{c,1}(\boldsymbol{x})$ (dashed). Right graph: Observer error converging to zero for the linearly unstable nonlinear plant.

VI. Simulations With Nonlinear Model

A. Observer

If we are using an observer for state estimation only, without a controller that suppresses vortex shedding, the observer must incorporate the *nonlinearities* in the system (in the same manner as an extended Kalman filter), in addition to linear output injection designed by the backstepping method. Including the nonlinear term in (1), the plant model (4) in the (ρ, ι) coordinates is

$$\begin{aligned}\rho_t &= a_R\rho_{xx} + \left(b_R(x) + c_R(x)\left(\rho^2+\iota^2\right)\right)\rho - a_I\iota_{xx} \\ &\quad - \left(b_I(x) + c_I(x)\left(\rho^2+\iota^2\right)\right)\iota \qquad (71)\\ \iota_t &= a_I\rho_{xx} + \left(b_I(x) + c_I(x)\left(\rho^2+\iota^2\right)\right)\rho + a_R\iota_{xx} \\ &\quad + \left(b_R(x) + c_R(x)\left(\rho^2+\iota^2\right)\right)\iota \qquad (72)\end{aligned}$$

for $x \in (0,1)$, where $c_R(x) = \Re(a_4)\exp(-r(x))$, $c_I(x) = \Im(a_4)\exp(-r(x))$, and $r(x) = \Re\left((1/a_1)\int_{x_d}^{(1-x_d)x+x_d} a_2(\tau)\,d\tau\right)$. The leftmost graph in Fig. 1 shows the open-loop plant response for the nonlinear system for $x_d = -7$, at Reynolds number $Re = 60$.[3] (Only ρ is shown; ι looks qualitatively the same). The system is linearly unstable and goes into a quasi-steady/limit-cycling motion reminiscent of vortex shedding. The middle graph of Fig. 1 shows the output injection gains (47). The observer consists of a copy of (71)–(72) with linear output injection given by (47) in terms of the state feedback gains, which are computed using (20)–(24). The rightmost graph in Fig. 1 shows the convergence of that observer, despite the plant undergoing unsteady motion, governed by a linear instability and kept bounded by the cubic nonlinearities.

B. Output-Feedback Controller

The left graph in Fig. 2 shows the feedback gain kernels, $k_x(1,y)$ and $k_{c,x}(1,y)$, used in (49)–(50). It is interesting to notice the similarity with the middle graph of Fig. 1, which is due to the definition of output injection gains in terms of state feedback gains in (47), and the fact that $a_I = 0$ in this numerical example. When a stabilizing controller is present, simulations show that one can use either a linear or a nonlinear observer. The middle graph in Fig. 2 shows the closed-loop response with a nonlinear observer. Although our controller (49)–(50) is linear, it is easy to understand why it is stabilizing for large initial conditions (the i.c.'s of the uncontrolled vortex shedding). This is due to the nonlinearities being cubic *damping* terms, which have a stabilizing effect on large states. The ability of our linear controller to stabilize vortex shedding is in agreement with recent results by Lauga and Bewley [10], where linear $\mathcal{H}_2/\mathcal{H}_\infty$ optimal control methods were used for a spatially discretized Ginzburg–Landau model, and stabilization was achieved up to $Re = 97$. Their controller is structurally similar to ours—a linear state feedback controller plus an observer consisting of a copy of the nonlinear system and linear output injection. The difference is twofold: Our design is for the continuum model and it places both the sensor(s) (in addition to the actuator(s)) on the bluff body. It was pointed out in [10] that stabilization becomes increasingly difficult when the Reynolds number and the number of open-loop unstable modes is increased, as these unstable modes become nearly uncontrollable and unobservable. When designed for the exact Reynolds number of the plant, our controller with nonlinear observer stabilizes the nonlinear plant (71)–(72) up to $Re = 127$. A controller designed for $Re = 60$, stabilizes the nonlinear plant up to $Re = 78$, while a controller designed for $Re = 80$ stabilizes the nonlinear plant up to $Re = 88$. This indicates some degree of robustness. The right graph in Fig. 2 shows the closed-loop response when a linear observer is used, and the controller is applied to the linearized plant. This is exactly the case proven mathematically in the previous sections, and the states converge to zero as expected.

C. A Fully Linear Compensator

As mentioned above, simulations show that either a nonlinear or a linear observer suffices in the presence of a stabilizing controller. When the observer is linear one can take a Laplace transform of the observer and get a transfer function of the linear compensator. The compensator is two-input–two-output, however due to the symmetry in the plant, only two of the four transfer functions are different. Fig. 3 shows the Bode plots of the transfer function of the linear compensator, as well as the stable closed-loop response of the nonlinear plant under the linear compensator. The linear compensator can be approximated very accurately with a 10th order reduced model, which is stable and minimum phase.

D. An Alternative Actuator/Sensor Architecture

In Fig. 3, we used an opportunity to show that actuation/sensing can also be done in a Dirichlet–Neumann configuration (in addition to the Neumann/Dirichlet configuration used in Fig. 2). In this case we used the measurements of $y_R(t) = \rho_x(1,t)$ and $y_I(t) = \iota_x(1,t)$, the linear observer (28)–(29) with output injection gains

$$\begin{aligned}p_1(x) &= a_R k_1(x) + a_I k_{c,1}(x)\\ p_{c,1}(x) &= -a_I k_1(x) + a_R k_{c,1}(x)\end{aligned} \qquad (73)$$

[3]Defined as $\boldsymbol{Re} = \boldsymbol{\rho U_\infty D/\mu}$, where $\boldsymbol{U_\infty}$ is the free stream velocity, $\boldsymbol{D}$ is the cylinder diameter, and $\boldsymbol{\rho}$ and $\boldsymbol{\mu}$ are density and viscosity of the fluid, respectively. Vortex shedding occurs when $\boldsymbol{Re} > 47$.

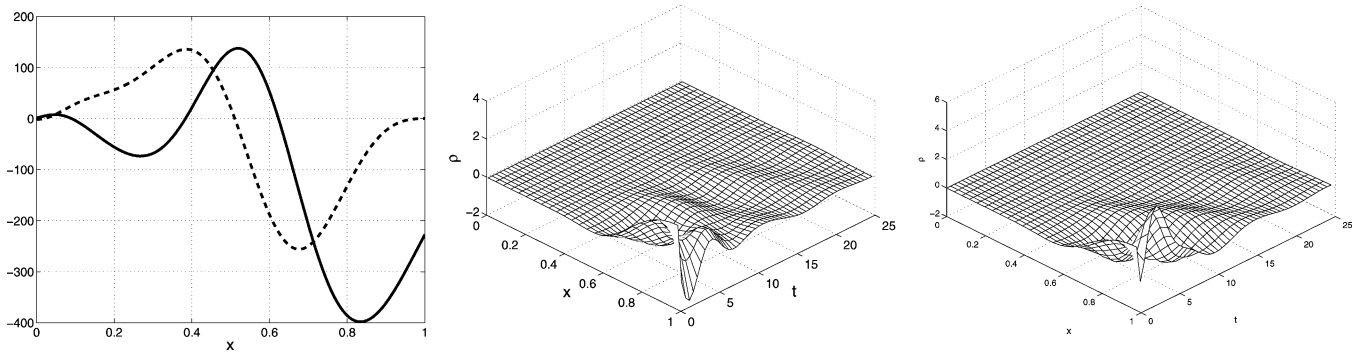

Fig. 2. Left graph: State feedback gain kernels $\boldsymbol{k}_x(\mathbf{1},\boldsymbol{x})$ (solid) and $\boldsymbol{k}_{c,x}(\mathbf{1},\boldsymbol{x})$ (dashed). Middle graph: Closed-loop response. Right graph: Closed-loop response for linear controller applied to linearized plant.

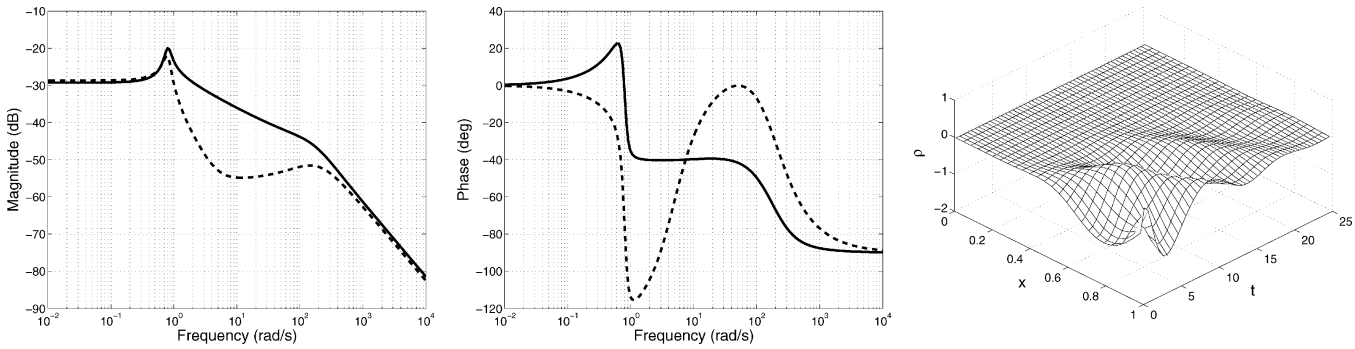

Fig. 3. Compensator transfer functions from $\boldsymbol{\rho}_x(\mathbf{1})$ to $\boldsymbol{\rho}(\mathbf{1})$ (solid) and $\boldsymbol{\iota}_x(\mathbf{1})$ to $\boldsymbol{\rho}(\mathbf{1})$ (dashed), and closed-loop plant response.

and actuation via $\rho(1,t)=\hat{\rho}(1,t)=u_R(t)$ and $\iota(1,t)=\hat{\iota}(1,t)=u_I(t)$. Fig. 3 shows the compensator Bode plots from $\rho_x(1)$ to $\rho(1)$ (solid line) and from $\iota_x(1)$ to $\rho(1)$ (dashed line).

REFERENCES

[1] O. M. Aamo and M. Krstić, "Global stabilization of a nonlinear Ginzburg–Landau model of vortex shedding," *Eur. J. Control*, vol. 10, no. 2, 2004.

[2] O. M. Aamo, A. Smyshlyaev, and M. Krstić, "Boundary control of the linearized Ginzburg–Landau model of vortex shedding," *SIAM J. Control Optim.*, vol. 43, no. 6, pp. 1953–1971, 2005.

[3] A. Balogh and M. Krstić, "Infinite dimensional backstepping-style feedback transformations for a heat equation with an arbitrary level of instability," *Eur. J. Control*, vol. 8, no. 2, pp. 165–176, 2002.

[4] A. Friedman, *Partial Differential Equations of Parabolic Type*. Upper Saddle River, NJ: Prentice-Hall, 1983.

[5] M. Gunzburger and H. C. Lee, "Feedback control of Karman vortex shedding," *Trans. ASME*, vol. 63, pp. 828–835, 1996.

[6] J.-W. He, R. Glowinski, R. Metcalfe, A. Nordlander, and J. Periaux, "Active control and drag optimization for flow past a circular cylinder: I. Oscillatory cylinder rotation," *J. Comput. Phys.*, vol. 163, pp. 83–117, 2000.

[7] P. Huerre and P. A. Monkewitz, "Local and global instabilities in spatially developing flows," *Annu. Rev. Fluid Mech.*, vol. 22, pp. 473–537, 1990.

[8] M. Krstić, I. Kanellakopoulos, and P. Kokotović, *Nonlinear and Adaptive Control Design*. New York: Wiley, 1995.

[9] E. Lauga and T. R. Bewley, "$\boldsymbol{H}_\infty$ control of linear global instability in models of non-parallel wakes," in *Proc. 2nd Int. Symp. Turbulence Shear Flow Phenomena*, Stockholm, Sweden, 2001.

[10] ——, "Performance of a linear robust control strategy on a nonlinear model of spatially-developing flows," *J. Fluid Mech.*, vol. 512, pp. 343–374, 2004.

[11] W. J. Liu, "Boundary feedback stabilization of an unstable heat equation," *SIAM J. Control Optim.*, vol. 42, no. 3, pp. 1033–1043, 2003.

[12] P. A. Monkewitz, private communication.

[13] D. S. Park, D. M. Ladd, and E. W. Hendricks, "Feedback control of a global mode in spatially developing flows," *Phys. Lett. A*, vol. 182, pp. 244–248, 1993.

[14] ——, "Feedback control of von Kármán vortex shedding behind a circular cylinder at low Reynolds numbers," *Phys. Fluids*, vol. 6, no. 7, pp. 2390–2405, 1994.

[15] A. Smyshlyaev and M. Krstić, "Closed form boundary state feedbacks for a class of 1D partial integro-differential equations," *IEEE Trans. Autom. Control*, vol. 49, no. 12, pp. 2185–2202, Dec. 2004.

[16] ——, "Output feedback boundary control by backstepping and application to chemical tubular reactor," in *Proc. Amer. Control Conf.*, Boston, MA, Jun.-Jul. 30–2, 2004.

[17] K. Roussopoulos and P. A. Monkewitz, "Nonlinear modelling of vortex shedding control in cylinder wakes," *Physica D*, vol. 97, pp. 264–273, 1996.